A continuous simulation approach for the estimation of extreme flood inundation in coastal river reaches affected by meso and macro tides

Sopelana J[1], Cea L[2], Ruano S[3]

[1] Aquática Ingeniería, Spain. jsopelana@aquaticaingenieria.com

[2] Environmental and Water Engineering Group, Departamento de Ingeniería Civil, Universidade da Coruña, Spain. luis.cea@udc.es. ORCID: 0000-0002-3920-0478

[3] Universidade da Coruña, Spain, silda.ruano@gmail.com

Abstract Considering the joint probability of occurrence of high sea levels and river discharges, as well as the interactions between these sources of flooding, is of major importance to produce realistic inundation maps in river reaches affected by the sea level. In this paper we propose a continuous simulation method for the estimation of extreme inundation in coastal river reaches. The methodology combines the generation of synthetic long-term daily time series of river discharge and sea level, the downscaling of daily values to a time resolution of a few minutes, the computation of inundation levels with an unsteady high-resolution two-dimensional model and the use of interpolation techniques to reconstruct long-term time series of water surface from a limited number of characteristic cases. The method is especially suitable for small catchments with times of concentration of a few hours, since it considers the intradiurnal variation of river discharge and sea level. The methodology was applied to the coastal town of Betanzos (NW of Spain), located at a river confluence strongly affected by the sea level. Depending on the return period and on the control point considered, the results obtained with the proposed methodology show differences up to 50 cm when compared with the standard methodology used in this region for the elaboration of flood hazard maps in accordance with the requirements of the European Directives. These results indicate the need for adaption of the standard methodology in order to produce more realistic results, and a more efficient evaluation of flood hazard mitigation measures.

Keywords Extreme flooding; Coastal river reach; Continuous simulation; Macrotidal estuary; 2D flood inundation modelling

1 Introduction

Flooding in coastal river reaches can be affected by different hydrologic and oceanographic extreme events, as high river discharges, large ocean waves, astronomical spring tides, storm surges and local rainfall intensities. The simultaneous occurrence of two or more of these sources of flooding is often the cause of the highest inundation levels registered in coastal cities and makes them particularly vulnerable to flooding. The joint probability of extreme sea levels and waves in coastal areas has been the subject of several studies (Mazas and Hamm 2017; Garrity et al. 2006; Hawkes 2008; Hawkes et al. 2002; Hanson et al. 2008; van Gelder et al. 2004; Wadey et al. 2015). On the other hand, the literature is much scarcer regarding the combined effects of extreme sea levels and river discharges in coastal river reaches, which is the case studied in this paper. The most relevant published studies are those of (van der Made 1969; Acreman 1994; Svensson et al. 2002; Hawkes 2003; Svensson et al. 2004; Zhong et al. 2013; Petroliagkis et al. 2016). Despite these references, most of the flood hazard studies that are undertaken in coastal areas do not account properly for the probability of simultaneous occurrence of extreme sea level and river discharge (Thieken et al. 2006; Archetti et al. 2011). In practice, extreme events are either assumed to be independent or an arbitrary combination of return periods is used (Teakle et al. 2005; Webster et al. 2014). However, if input variables are assumed to be independent, the likelihood of flooding will be considerably underestimated (White 2007). On the other hand, assuming total dependence will produce too conservative flood levels for a given return period, leading to an over-design of flood defences.

Taking into account sea level and river discharge as the sources of flooding in coastal river reaches has two major implications. First, a given water level can result from different combinations of sea level and river discharge. Hence, the water level probability density function (pdf) will be determined by the probability of occurrence of the ensemble of these combinations. This gives place to different possibilities in the identification and sampling of extreme events (Mazas and Hamm 2017) and makes the estimation of the water level pdf much more complex than in a typical univariate problem (van der Made 1969; Acreman 1994;

Zhong et al. 2013). The second implication is that the correlation between the sea level and the river discharge might be not negligible (Acreman 1994; Zhong et al. 2013), since the storm surge and the surface runoff are the consequence of severe regional meteorological events. In that case, a statistical analysis of concurrent extreme events must be performed to estimate their joint pdf, which is often complicated due to the lack of simultaneous time series of enough length.

Temporal dependence may also be a relevant issue in an extreme value analysis. Attending to the time scale, Hawkes (2008) distinguishes three types of temporal correlations that might be considered: short-term autocorrelation (Cai et al. 2007, 2008), short-term seasonality over one year and long-term trend due to climate change. Natural climate variability related to global atmospheric circulation patterns with time scales from a few years to decades, as the North Atlantic Oscillation (NAO) or the Atlantic Multidecadal Oscillation (AMO), can also have an effect on the long-term autocorrelation between the river discharge and the surge. Despite its relevance, temporal dependence is not considered in most extreme flood inundation studies.

The most straightforward approach to account for the correlation of sea level and river discharge is the so-called historical reconstruction method (Acreman 1994), also called hindcast. With this approach, the time series of water level at a given location are reconstructed from historical simultaneous records of the boundary variables, using for that purpose either the so-called structure functions (Petroliagkis et al. 2016), or a continuous simulation with a numerical model. Once the historical time series of water level have been reconstructed, maximum water levels are extracted and a univariate extreme distribution can be fitted to the data. The main advantage of this approach is that the statistical dependence between input variables does not need to be explicitly analysed. However, this method is not often used because the results are limited by the length of the historical input records, and it might be time consuming if a continuous simulation is performed with a complex numerical model.

Another approach to consider the combined effect of several variables is the so-called joint probability approach (Hawkes 2008). In this kind of methods, the joint pdf of the forcing variables must be estimated from the available data records. This can become rather complicated if the variables are correlated, and it is the reason why in practice only two variables are often considered (Hawkes et al. 2008). Once the joint pdf has been estimated, it must be integrated over all the possible combinations of the input variables that cause a water level higher than a given value, in order to compute its probability of exceedance. To do so, a numerical flood model is often used to map the input variables into water levels. This brings up an additional problem, since the numerical integration of the joint pdf requires many model runs, implying high CPU times. Zhong et al. (2013) used 30.000 model runs, and in order to keep the CPU times affordable they were obliged to run an extremely simplified 1D inundation model.

In this paper, we propose a continuous simulation method for the estimation of extreme inundation in coastal river reaches affected by the sea level. The innovation point of the methodology presented here is the combination of three techniques to account for different sources of flooding. First, the generation of long-term (several hundred years) synthetic time series of the flooding variables (in our case sea level and river discharge), accounting for their seasonal variability and possible correlations between variables. Second, the computation of inundation maps with a high-resolution 2D hydraulic model in order to account for the interaction between the different sources of flooding. And third, the application of interpolation techniques to reconstruct long-term time series of daily maximum water level from just a few characteristic values computed with the 2D numerical model. The advantage of the proposed methodology is that, through the combination of these three techniques, it allows to account simultaneously and in a natural way for the joint probability of occurrence of different sources of flooding and for their mutual interaction, as well as for the seasonal variability of the involved variables. The proposed methodology was applied to the coastal town of Betanzos, located at the confluence of the rivers Mandeo and Mendo in a macrotidal estuary in the North West of Spain. The results obtained show relevant differences to those obtained with the standard methodology used in this region for the elaboration of flood hazard maps in accordance with the requirements of the EU Directive 2007/60/CE, which indicates the need for adaption of the standard methodology in order to produce more realistic flood inundation results and a more efficient evaluation of flood hazard mitigation measures.

2 Methodology

The methodology proposed in this paper is based on the reconstruction of long-term time series of water levels (predictand) from simultaneous long-term time series of the variables involved in the flooding process (predictors). Here, we refer with long-term series to periods of several hundred years (500 years in the case study presented in section 3, but the methodology can be applied with time series of other lengths). This is done to overcome the problems related to the limited length of the data records in the historical

reconstruction methods. The time series of the predictors are used to define the boundary conditions of a numerical inundation model that solves the two-dimensional shallow water equations. Since the 2D numerical model is very expensive in terms of CPU time, a surrogate model based on the Maximum Dissimilarity Algorithm presented by Kennard et al. (1969) and on the Radial Basis Functions (RBF) interpolation technique (Franke 1982) is used to reconstruct a the long-term time series of daily maximum water levels from only a few characteristic cases computed with the 2D model. The use of a surrogate model implies a considerable reduction of CPU time. Once the water levels have been reconstructed, a univariate analysis is done to obtain inundation levels associated to any return period.

In estuaries the predictors are typically the river discharge and the sea level (Petroliagkis et al. 2016), which are the two sources of flooding considered in this paper. The relative importance of sea level depends on the astronomical tidal range and on the storm surge in the study area. In this regard, the first classification of shorelines by tidal range was proposed by Davies (1964), who defined macrotidal estuaries as those with a tidal range larger than 4 m and mesotidal coastlines as those with a tidal range between 2 and 4 m. This classification was later refined by Hayes (1979) as high-mesotidal (tidal range between 2 and 3.5 m), low-macrotidal (tidal range between 3.5 and 5 m) and macrotidal (tidal range higher than 5 m). In macrotidal coastlines with moderate surge levels, the effect of astronomical tide will be much more relevant in the flooding process than the storm surge. In mesotidal coastlines both effects might be relevant, while in microtidal estuaries the meteorological surge will be in general predominant.

The main steps of the proposed methodology are sketched in Fig. 1 and are described in the following of this section.

Fig. 1 Schematic representation of the main steps of the proposed methodology

First, the relevant predictors are defined at a daily scale. River discharge and sea level are time dependent variables that vary at different time scales. While the tidal cycle in most coastal areas is diurnal or semidiurnal, the duration of a flood hydrograph can vary from a few hours to several days depending on the concentration time of the river basin. The proposed methodology works in the first place with daily values of both predictors in order to analyse their long-term variability. At this step, the river discharge is represented by its daily mean (Q_d), which is the most commonly available value. If the daily maximum discharge (Q_p) is available, it can also be used as a predictor instead of the daily mean value. The sea level at a daily scale is represented by the astronomical tidal range (TR) and by the mean daily storm surge (S_d). Taking into account that the sea level and river discharge vary in an intradiurnal time scale, the time lag between their daily peak values (T_{lag}) must also be considered as a predictor, since the simultaneous occurrence of the peak discharge and the high tide can have a relevant effect in the maximum inundation levels (Hughes et al. 2001). This is especially important in small rapid response catchments with times of concentration of a few hours.

The second step of the methodology is the generation of long-term time series of the predictors with a daily time resolution. The modeller must find an appropriate technique to generate synthetic time series of Q_d, TR, S_d and T_{lag} at the specific study site. At this step it is convenient that the synthetic time series reproduce the seasonal variability in the predictors. This is especially important for the river discharge and storm surge, which usually have non-negligible seasonal variability. In this way, it is implicitly considered that the probability of simultaneous occurrence of extreme tides with peak discharges varies along the year. Possible correlations between the predictors should also be analysed and, if relevant, included in the time series generation algorithm. These correlations might include S_d-TR and S_d-Q_d dependencies. Surge-tide interactions are more likely to happen in shallow coastal areas, because the surge generated by the wind depends on the water depth and therefore, on the tide level. In deep coastal areas the water depth difference between high and low tide is not significant compared to the total depth and therefore, the wind-generated surge is barely correlated to the tide level.

Once the long-term daily time series of the predictors are generated, a relatively small number of representative days are sampled in the third step of the methodology. An efficient data mining technique should be used in order to extract the maximum information of the time series from just a small number of characteristic cases. Several clustering algorithms are available to perform this task, as the k-means, the Self-organizing Maps or the Maximum Dissimilarity Algorithm. The number of characteristic days will depend on the number and variability of the predictors considered in the analysis, and in the efficiency of the reconstruction algorithm used in the step 6 of the methodology. Nevertheless, it is important to keep the number of characteristic cases as small as possible in order to reduce the computational time in step 5 of the methodology.

Since river discharge and sea level vary significantly within a day, their daily values must be downscaled to a higher time resolution. This is done in the fourth step of the methodology. The daily variation of storm surge has not been considered in this work since in macro tidal estuaries its daily variability is less relevant and much more difficult to characterize than that of the astronomical tide. A time resolution of 15 minutes is in general small enough to capture accurately the variability of the astronomical tide and of the river discharge in urban flood studies. The tidal range can be easily downscaled using the tidal harmonic constituents at the study site, which are generally available from any tidal gauge. The river discharge can be downscaled using a dimensionless unit hydrograph. The choice of a unit hydrograph is case specific, and must be done through a previous analysis of several flood hydrographs registered in the hydrological basin of the study site. A possible choice is the Soil Conservation Service unit hydrograph, which depends on two parameters: the peak discharge (Q_p) and the time to peak (T_p). Several methods to estimate T_p and Q_p based on mean daily data and on the hydrological characteristics of the basin are available in the literature (Fuller 1914; Ellis et al. 1966; Taguas et al. 2008; Dastorani et al. 2010).

In the fifth step, a high-resolution two-dimensional model is used to compute the inundation maps in the characteristic days selected in step 3. The downscaled sea level and discharge hydrographs computed in step 4 are used as boundary conditions in the numerical model. Notice that only the characteristic days selected in step 3 are modelled in order to avoid excessively long computation times. The desired outputs of the model are the flood extension and the daily maximum water depths at several control points. Other predictands, like the water velocity, can also be used to assess flood hazard.

The sixth and last step of the proposed methodology is the reconstruction of long-term time series of daily maximum water level at the control points from the results of the 2D numerical model in the characteristic days. In order to do so, an interpolation technique for multidimensional scattered data is used. In this work we have used the Radial Basis Function interpolation technique, although other alternative methods might be used. RBF interpolation techniques consist on a weighted sum of radially symmetric basis functions located at the data points. In our case, the data points correspond to the characteristic cases, defined by Q_d, TR, S_d and T_{lag}. There are several basis functions which can be used (linear, cubic and Gaussian, among others), most of which are defined by a shape parameter that influences the domain of attraction of each data point. In the present work we have implemented the algorithm presented in (Rippa 1999) for choosing an optimal value of the shape parameter. This algorithm has proved to be a powerful technique to reconstruct time series of sea state parameters (Camus et al. 2011a, Camus et al. 2011b).

After applying the previous six steps we obtain, at each control point, a 500 years long time series of daily maximum water levels. From this long-term time series, return periods can be estimated using a simple plotting-position formula without fitting any probabilistic law. This kind of direct estimation is robust for return periods lower than the length of the reconstructed time series (say up to 250 years for a 500 years long time series), but should be used with care for return periods corresponding to the time series duration.

3 Study case

3.1 Case description

The methodology described in section 2 was applied to the coastal town of Betanzos (NW Spain), located at the confluence of the rivers Mandeo and Mendo, in the inner part of the estuary of Betanzos (Fig. 2). The river Mandeo is 50 km long and its watershed has an area of 350 km^2. Its main tributary is the Mendo river, which is 30 km long and has a catchment area of 100 km^2. The estuary of Betanzos is about 7 km long and 1 km width. With a spring tidal range of roughly 4.5 m, it can be classified as a macrotidal estuary according to the classification given by Davies (1964). Surge levels are moderate in magnitude, the maximum values of surge registered being of the order of 40 cm. In a global classification of coastal flood hazard climates presented recently in Rueda et al. (2017), the NW part of Spain was classified as a macrolevel tide-dominant region, with an average relative contribution of astronomical tide to the annual maxima of sea level above 80%. Therefore, the inundation levels in the town of Betanzos are strongly influenced by the sea level, and specially by the astronomical tide rather than by the storm surge. Nevertheless, both were considered in this study, in addition to the river discharge.

Fig. 2 Betanzos estuary (top). Map of Betanzos city in the 14th century (Colón 2012) (bottom-left) and schematic representation of the urbanisation and land uses in 2016 (bottom-right)

Historical flooding problems have been reported in the town of Betanzos since 1584 (PEPC 2002). The lowest part of the town, which lies near the Mandeo river floodplains (Fig. 2), is flooded almost every year

when spring tides occur simultaneously with high river discharges. The problem was exacerbated by the urbanisation of the floodplains in the 20th century and the construction in 1906 of a narrow artificial channel downstream the confluence (Fig. 2). Nowadays, a train embankment crosses the estuary and the Mendo's floodplains have been transformed into industrial areas, which further limit the discharge capacity of the river.

3.2 Available data

Close to Betanzos, there is a tide gauge that belongs to the port of A Coruña. The available sea level data in that gauge covers the period from 1992 to 2016. From these data, the tidal harmonic constituents and the daily storm surge were extracted by Pérez-Gómez (2014) and used in this work.

Regarding discharge data, there are two gauging stations. The first one is located in the river Mandeo, 30 Km upstream the town of Betanzos, and it covers 31 years of mean daily discharge data. It also provides instantaneous discharge data during the last 8 years. The second gauging station is located in the tributary river Mendo, 10 Km upstream of Betanzos, and it covers a period of 8 years of instantaneous discharge data.

3.3 Seasonality and correlations between predictors

As mentioned before, when generating the synthetic long-term time series, it is necessary to account for seasonality and possible correlations between the predictors. Before embarking on a complex multivariable analysis, it is useful to undertake a cross-correlation analysis for any relevant variable pairs in order to consider just the most relevant correlations (Hawkes 2003). The existence and strength of these correlations is case dependant and must be analysed from the available historical field data. In the case study presented here, the four predictors considered are the river discharge (Q_d), the astronomical tidal range (TR), the storm surge (S_d) and the time lag between peak discharge and high tide (T_{lag}).

The time lag between peak discharge and high tide is fully independent from the other predictors, since there is no relation at all between the tidal phase and the shape of the rainfall runoff hydrographs. The three possible correlations between variable pairs to be analysed are therefore: TR-Q_d, TR-S_d and S_d-Q_d.

The astronomical tide is deterministic and mostly independent from the river discharge. Actually, there is a slight dependency between these two variables due to the seasonality of the processes that generate them. The spring tidal ranges are higher near the equinoxes, while the maximum river discharges in the study catchment are higher around the winter solstice (Fig. 3). This is not a direct cause-effect correlation, and it only implies that the probability of having simultaneous high values of discharge and tidal range differs from one month to another. In fact, the correlation coefficient between daily values of tidal range and river discharge is just 0.01. This effect is considered in the proposed methodology, since the synthetic time series of these predictors account for seasonality.

Fig. 3 Monthly average and standard deviation values of daily tidal range (top-left), mean daily discharge (top-centre) and mean daily storm surge (top-right), and correlations between these predictors at daily scale (bottom)

Regarding tide-surge correlation, the storm surge might depend on the tidal level at certain shallow coastal regions. This is because the surge generated by the wind depends on the water depth and therefore, on the tidal level. In the NW of Spain the storm surge is mainly generated by low atmospheric pressure, rather than by wind shear stress and therefore, the tidal influence is not relevant. In addition, in the coastal waters of NW of Spain the water depth difference between high and low tide is not significant compared to the total depth. For these reasons, in the study case presented here the surge is not correlated to the tide level (Fig. 3). The historical records of storm surge and tidal range show a correlation coefficient of 0.005. Hence, surge-tide interactions have not been considered in the generation of the synthetic time series.

Surge-discharge correlations are more likely to occur in this region, since both phenomena are dependent on the weather conditions. A storm event brings heavy rains and strong winds, which might produce at the same time high values of river discharge and surge. Fig. 3 shows simultaneous daily values of discharge and surge registered between 1992 and 2016, together with those corresponding to the synthetic data. There is a slight trend in the historical data, especially for high values of discharge, although the correlation coefficient is low (0.21). If the correlation between discharge and surge is computed on a monthly basis, larger

correlation coefficients are found in autumn, winter and spring, while in summer the correlation is lower (Fig. 4).

Fig. 4 Correlation coefficient between Q_d and S_d computed on a monthly basis (left), Q_d-R_d scatter plot for the months of January (centre) and June (right). Values computed from historical and synthetic data are shown in blue and red respectively

3.4 Long-term time series

The available simultaneous field measurements of Q_d, TR and S_d cover only a few years (from 1992 to 2016). From these, 500 years-long synthetic time series of river discharge and sea level were generated in order to obtain a statistically representative data set that considers seasonality and possible correlations between predictors.

Sea level time series were generated from the tidal harmonic constituents, with a time resolution of 15 minutes. From these, the TR was extracted every 24 h as the difference between two consecutive relative minimum and maximum values. The synthetic time series of TR account for seasonality, as shown in Fig. 3.

The time series of Q_d for the Mandeo river were obtained from a regression hydrological model developed by IH Cantabria (2014) to define flood hazard maps in accordance with the requirements of the EU Directive 2007/60/CE. The regression model simulates synthetic values of Q_d at a particular river reach, based on the following climate and catchment descriptors: mean annual precipitation, catchment area, mean catchment slope and mean SCS curve number. The model was fitted to measured data at 18 gauge stations in the hydrographic region where the river Mandeo is located (Galicia Costa, NW of Spain, 13000 km^2). The synthetic time series of Qd account for seasonality, with largest and smallest values occurring respectively at the winter and summer solstices (Fig. 3).

Regarding Mendo's discharge, its value is highly correlated with the Mandeo's discharge, with a correlation coefficient of 0.80 (Fig. 5). Hence, a power regression model was fitted based on the available historical data at the gauging stations. The coefficient of determination of the power regression model is R^2=0.86. A random noise (ξ) was added to the regression model in order to reproduce the real correlation between the two time series:

$$Q_{d,Mendo} = 0.469 \cdot {Q_{d,Mandeo}}^{0.715} + \xi \quad (1)$$

This regression model was used to generate the simultaneous Mendo's discharge from the synthetic Mandeo's Q_d time series. The synthetic data reproduces correctly the observed dispersion between the observed discharges (Fig. 5). It should also be noticed that the magnitude of the Mendo's discharge is about an order of magnitude lower than the Mandeo's discharge and therefore, it has a minor influence in the inundation levels.

Fig. 5 Regression between the observed mean daily discharges at the gauging stations of the Mandeo (Qmandeo) and Mendo (Qmendo) rivers. The synthetic values of the Mendo discharge computed from Equation (1) and the fitted power regression are also shown

As mentioned in section 3.3, the storm surge is slightly correlated with the river discharge, and this must be considered when generating the S_d synthetic time series. In order to take into account at the same time the seasonality and the monthly correlation between Q_d and S_d, the following procedure was followed. First, the synthetic time series of Q_d was normalized as:

$$Q^* = \frac{Q_d - \mu_{Q_d}}{\sigma_{Q_d}} \quad (2)$$

where Q^* is the normalized daily discharge, μ_{Q_d} is the average daily discharge and σ_{Q_d} is the standard deviation of the daily discharge. Both μ_{Q_d} and σ_{Q_d} were computed on a monthly basis from the synthetic time series, i.e. their value depends on the month considered, as shown in Fig. 3. Then, the normalized discharge was correlated with random samples (Z) generated from a standard Gaussian distribution as:

$$t = \rho\, Q^* + \sqrt{1-\rho^2}\, Z \quad (3)$$

where Z is a random variable following a standard normal distribution (with zero mean and unit standard deviation), and ρ is the observed correlation between the discharge and the storm surge, computed on a monthly basis from the historical time series of daily data. The values of ρ for each month are plotted in Fig. 4. Finally, the synthetic values of S_d are computed as:

$$S_d = \mu_{S_d} + t\,\sigma_{S_d} \tag{4}$$

where μ_{S_d} and σ_{S_d} are respectively the observed mean and standard deviation of the daily surge, computed form the historical time series (from 1992 to 2014) on a monthly basis. Their values are shown in Fig. 3.

The previous procedure produces synthetic time series that reproduce the observed seasonality and correlations between the Q_d, S_d and TR, as shown in Figs. 3, 4.

Finally, the synthetic series of T_{lag} was generated as a random value between 0 and 12.42 hours with a uniform distribution, since the astronomical tidal level and the river hydrographs are completely uncorrelated and have the same probability of occurrence at any time within the day.

3.5 Selection of characteristic days

The Maximum Dissimilarity Algorithm was used to select a small number of characteristic days from within the long-term daily time series of Q_d, TR, S_d and T_{lag}, which are the four predictors considered in the analysis. Each characteristic day corresponds to one day of the synthetic time series, and represents a combination of simultaneous values of the four predictors considered.

In order to determine the required number of characteristic days, a simple sensitivity analysis was performed applying the methodology with 30, 40, 50 and 60 characteristic days. The results obtained with 40, 50 and 60 days were not significant and therefore, 40 characteristic days were chosen for this study case.

3.6 Downscaling

The daily values of discharge and tidal range obtained from the synthetic time series cannot be directly used in an unsteady urban inundation model, because these models work at a much higher time resolution. River discharge and sea level must be downscaled to impose the boundary conditions in the 2D inundation model. Downscaling is only undertaken on the 40 characteristic cases, since these are the only cases that will be computed with the numerical model.

The daily mean river discharge was downscaled using the SCS unit hydrograph, which requires only two parameters: the peak discharge (Q_p) and the time to peak (T_p). The peak discharge was derived from the mean daily discharge. For that purpose, eight years of instant flow data were used to define a 2-branch power regression with a global coefficient of determination R^2=0.88 (Fig. 6). The 2-branch power regression found is given by:

$$Q_p = 0.782 \cdot {Q_d}^{1.1652} \quad if \quad Q_d \geq 20 m^3/s \tag{5}$$
$$Q_p = 1.858 \cdot {Q_d}^{0.8394} \quad if \quad Q_d < 20 m^3/s$$

This regression was used to compute Q_p from Q_d on a daily basis.

Fig. 6 Relation between Q_p and Q_d at Mandeo gauging station (left). The fitted 2-branch power regression curve is shown as a solid line. Comparison between measured and estimated SCS hydrographs at the Mandeo gauge station for a flood event (right)

In order to define the time to peak the formula proposed by Robson and Reed (1999) was used:

$$T_p = 283 \cdot S_m^{-0.33} \cdot P_m^{-0.54} \cdot L_m^{0.23} \cdot (1+U)^{-2.2}$$

where T_p is the time to peak in hours, S_m is the mean stream slope, L_m is the mean stream length in km, P_m is the mean precipitation depth in the watershed expressed in mm, and U is the percentage of urban areas in the basin expressed as a decimal. The estimation given by Robson and Reed's formula was compared to the time to peak derived from field data measured at the Mandeo and Mendo's gauging stations during several flood events, showing a better agreement than other well-established formulas as those of Témez

(1991) and Kirpich (1940). The synthetic hydrograph computed in this way was compared to the measured one for certain flood events, showing a good general agreement, especially in the rising limb (Fig. 6).

Regarding astronomical tide, the intradiurnal variability of the sea level was defined from the astronomical tidal range, assuming a tidal period of 12.42 hours, which corresponds to the M2 harmonic constituent.

The intradiurnal variability of the storm surge was neglected and thus, its value was considered constant over one day. This approximation was assumed after an analysis of the mean (S_d) and maximum (S_{max}) daily values of surge registered at the tidal gauge. The hystorical records observed between 1992 and 2016 show a negligible intradiurnal variability of the storm surge, and a strong linear correlation between S_d and S_{max}, given by the equation $S_{max} = 1.05S_d + 0.05$ $(R^2 = 0.94)$.

3.7 Numerical model

The 40 characteristic cases were modelled with the software Iber (Bladé et al. 2014), which solves the 2D depth-averaged shallow water equations in order to compute the water depth and the two horizontal components of the depth-averaged velocity. The shallow water equations are solved with an unstructured finite volume solver explicit in time, which implements the scheme of Roe (1986) for the discretisation of the convective flux terms and an upwind discretisation of the topography (Bermúdez et al. 1998). The algorithms implemented in the model have been extensively validated and applied in previous studies related to river inundation and tidal currents in estuaries (Bladé et al. 2014b; Bodoque et al. 2016; Cea et al. 2015; Cea and French 2012; Fraga et al. 2016; Fraga et al. 2017; Garrote et al. 2016).

Fig. 7 shows the spatial domain included in the numerical model. It includes the confluence of the rivers Mandeo and Mendo, the city of Betanzos, and it extends over the whole estuary in order to impose the sea level condition at the open sea boundary. The finite volume mesh used in the computations has 126,266 elements with an average size of 11.5 m. In order to resolve properly the flow field in the urban area, the mesh resolution in the river confluence and in the urban area is higher, with a mesh size of the order of 5.7 m. In the outer estuary the mesh size is of the order of 50 m, which is large enough to propagate the tidal wave from the open sea to the river confluence.

Fig. 7 Spatial domain included in the 2D inundation model, including the confluence of the rivers Mandeo and Mendo, and the estuary of Betanzos. Imposed boundary conditions are also shown schematically. Control points (bottom-left) and detail of the numerical mesh (top-left)

A high accuracy Digital Surface Model (DSM) that integrates the river and estuary bathymetries with LIDAR terrain data was used to define the topography of the numerical model. A spatially variable Manning coefficient was defined from a land use chart. Six different land uses were defined with Manning values ranging from 0.02 in the main river channels to 0.15 in the residential areas.

The model was run for each of the 40 characteristic cases, using the downscaled discharge and sea level as the upstream and open sea boundary conditions respectively. A spin-up time of two days (circa four tidal cycles) was used to generate realistic initial conditions.

3.8 Water level reconstruction

In order to analyse the model results, 12 representative control points distributed along the Mandeo and Mendo rivers were defined (Fig. 7). The location of the control points was chosen in order to sample regions with a different exposure to the sea level influence. The RBF interpolation method was applied independently at each control point. The results of maximum water level obtained from the numerical model in the 40 characteristic days and the long-term time series of the four predictors (Q_d, TR, S_d and T_{lag}) were used to reconstruct the long-term time series of maximum daily water level at each control point by applying the Radial Basis Function technique. The proposed methodology is able to reconstruct the time series of water level simulating only a reduced number of cases.

From the 500-year reconstructed time series, the probability of exceedance of a given water level can be easily computed using a simple plotting position formula and without the need of fitting any statistical distribution for return periods up to circa 250 years. For larger return periods the reconstructed time series should be longer. In this case, we have used the plotting position formula proposed by Yu and Huang (2001) for a Gumbel distribution, although other alternative formulas might be used.

4 Results and discussion

The results obtained with the proposed methodology were compared with those obtained with the standard methodology used to evaluate flood hazard in the NW of Spain, which assumes the same return period for the river discharge and the sea level. Without a joint probability assessment, it is not possible to determine the probability of occurrence of such a conservative scenario. It could be one hundred years if the river flow and the sea level were fully dependent, or in excess of three million years if fully independence and one-day duration events are assumed (Hawkes 2008). In addition, there are several combinations of discharge and sea level that give the same inundation. For instance, a discharge higher than the 100-year discharge combined with a sea level lower than the 100-year sea level can produce the same hazard as the combination of the 100-year discharge and sea level.

Using the same numerical model, the maximum water level for three return periods (2.33, 100 and 500 years) was evaluated with the standard methodology, i.e. combining the river discharge and water level associated to the same return period. As expected, for a given return period the water levels calculated with the proposed methodology are lower than those computed with the standard methodology. Differences are higher at the control points which are closer to the river mouth (control points 1 and 2), and decrease as we move upstream. This is because the tidal influence decreases with the distance of the control point to the open sea. As the tidal influence disappears, the water depth becomes dependent solely on the river discharge, and in such a case both the proposed and the standard methodologies converge to the same results.

At control point 1 (Fig. 8) the 2.33-year water level computed with the standard methodology is 2.7 m referred to the Spanish datum (Mean Sea Level at the Alicante tidal gauge in Spain), while the same water level has a return period of 10 years according to the proposed methodology. Differences of the same magnitude are found at control points 2 and 3, which are located downstream the confluence of both rivers. At control points located further upstream the difference is lower, but still relevant especially in the Mandeo (Table 1). The standard methodology is therefore extremely conservative since it assumes total dependence between extreme values of sea level and river discharge. As shown in Fig. 8, differences between both methodologies are even more significant for higher return periods (100 and 500 years) since it is extremely unlikely that the 100-year sea level occurs the same day as the 100-year river discharge.

Fig. 8 Water levels referred to the Mean Sea Level at the Alicante tide gauge (Spain) for different return periods computed with the proposed methodology at control points 1, 3, 9 and 12. The water levels computed with the standard methodology for the return periods of 2.33, 100 and 500 years are also shown

The differences in the extension of the inundation computed with the proposed and the standard methodologies is shown in Fig. 9. As expected, the standard methodology overestimates the extension of the inundation when compared to the proposed approach. The extent of the tidal influence depends on the bed topography, tidal range and river discharge, and is therefore problem dependent. An interesting feature of the methodology is that, using a high accuracy numerical model, it is able to detect automatically the extension of the tidal influence and therefore the importance of the interaction between sea level and river discharge in the inundation levels. Fig. 10, which plots a longitudinal profile along both rivers for the 100-year return period water level computed with both methodologies, shows how the influence of the sea level on extreme flood inundation decreases as we move upstream the river reaches and far away from the river mouth.

Fig. 9 Inundation maps for the return period of 2.33 years computed with the proposed methodology (light blue) and with the standard methodology (dark blue)

Fig. 10 Longitudinal profile along the rivers Mendo and Mandeo of the 100-year return period water level computed with the proposed and the standard methodologies

Without a reconstruction technique, the unsteady 2D model would have to be run for every day during 500 years (circa 180.000 model runs), which at the present time is untenable considering the CPU requirements. Thus, the proposed methodology relies on the use of the RBF interpolation technique to reconstruct the water level time series over a long period of time from just a few model runs. The results are therefore

dependent on the accuracy of the reconstruction technique. In order to validate the time series reconstruction methodology, we have performed a comparison between the results obtained with the RBF interpolation and those computed with the numerical model. Twenty days of the reconstructed long-term water level time series were selected randomly and numerically modelled. The comparison between the numerical and the reconstructed results shows a good agreement, with R squared values that vary between 0.91 and 0.98 at the different control points (Fig. 11). The value of R^2 increases upstream, where the maximum water levels depend mainly on the river discharge and are not very sensitive to the tidal flow.

Fig. 11 Validation of the water level reconstruction methodology (Radial Basis Function). Water levels simulated with the numerical model Iber and reconstructed with the RBF technique at control points 8 (left) and 9 (right) for 20 validation cases

5 Conclusions

The methodology proposed in this paper to evaluate extreme inundations in rivers affected by meso and macro tides combines the generation of long-term synthetic time series of river discharge and sea level with a daily resolution, the downscaling of daily values to a 15 minutes time resolution, the computation of inundation levels with an unsteady high-resolution two-dimensional numerical model, and the use of interpolation techniques to reconstruct long-term time series of water surface elevation from a limited number of characteristic days. The method is especially suitable for small rapid response catchments with times of concentration of a few hours, since it considers the intradiurnal variation of river discharge and sea level. In case of bigger catchments, the relevant time scale should be defined, and the methodology should be adapted accordingly.

The method relies strongly in the ability of the hydrologist to build realistic synthetic time series of the predictors, which should account for possible correlations between variables, short-term autocorrelations and seasonality. Special care must be taken with surge-discharge and surge-tide interactions that might occur at certain coastal areas and, if relevant in the study region, should be considered in the generation of the synthetic time series of the predictors. The downscaling of the mean daily discharge, and more precisely the correct evaluation of the time of concentration of the basin, can also have an important impact on the results, since it will determine the probability of simultaneous occurrence of high discharges and sea levels.

Using a high-resolution 2D model is also a key feature of the method in order to consider properly the interaction between different sources of flooding, in our case sea level and river discharge. However, the CPU time required by these models implies that a reconstruction technique based on an appropriate interpolation method must be used to build the long-term time series of water level. The method relies in the accuracy of the interpolation method. In this paper we used RBF, which proved to be able to reproduce correctly the model results after calibration with just a few characteristic cases (40 in our case study).

As other existing joint probability and continuous simulation approaches, the proposed method is expected to give more realistic and coherent results than the standard methodologies commonly used to compute flood hazard, which consider the simultaneous occurrence of sea levels and river discharges associated to arbitrarily defined return periods.

Acknowledgments The authors would like to acknowledge the Department of Water Planning Administration of the Galician Government (Xunta de Galicia) for providing the DSM of the Betanzos estuary, the data from the flow discharge gauging stations and the synthetic discharge series of the Mandeo river. The authors would also like to thank the Spanish harbour government agency “Puertos del Estado”, for the A Coruña tidal gauge data.

References

Acreman MC (1994) Assessing the joint probability of fluvial and tidal floods in the river-roding. J Inst Water Environ Manage 8: 490–496. https://doi.org/10.1111/j.1747-6593.1994.tb01140.x

Archetti R, Bolognesi A, Casadio A, Maglionico M (2011) Development of flood probability charts for urban drainage network in coastal areas through a simplified joint assessment approach. Hydrol Earth Syst Sci 15:3115–3122. https://doi.org/10.5194/hess-15-3115-2011

Bermúdez A, Dervieux A, Desideri JA, Vázquez-Cendón, ME (1998) Upwind schemes for the two-dimensional shallow water equations with variable depth using unstructured meshes. Computer Methods in Applied Mechanics and Engineering 155(1-2):49-72

Bladé E, Cea L, Corestein G, Escolano E, Puertas J, Vázquez-Cendón ME, Dolz J, Coll A (2014) Iber: herramienta de simulación numérica del flujo en ríos. Revista Internacional de Métodos Numéricos para Cálculo y Diseño en Ingeniería 30(1):1-10. https://doi.org/10.1016/j.rimni.2012.07.004 (In Spanish)

Bladé E, Cea L, Corestein G (2014) Modelización numérica de inundaciones fluviales. Ingeniería del Agua 18(1):68-79. https://doi.org/10.4995/ia.2014.3144 (In Spanish)

Bodoque JM, Amérigo M, Díez-Herrero A, García J-A, Cortés B, Ballesteros-Cánovas JA, Olcina J (2016) Improvement of resilience of urban areas by integrating social perception in flash-flood risk management. Journal of Hydrology 541:665-676. https://doi.org/10.1016/j.jhydrol.2016.02.005

Cai Y, Gouldby BP, Dunning P, Hawkes PJ (2007) A Simulation Method for Flood Risk Variables. 2nd IMA Intl Conf Flood Risk Assessment. Institute of Mathematics and its Applications, Southend, UK, pp 85–95

Cai Y, Gouldby B, Hawkes P, Dunning P (2008) Statistical simulation of flood variables: Incorporating short- term sequencing. Journal of Flood Risk Management 1(1):3-12. https://doi.org/10.1111/j.1753-318X.2008.00002.x

Camus P, Mendez FJ, Medina R (2011a) A hybrid efficient method to downscale wave climate to coastal areas. Coastal Engineering 58(9):851-862. https://doi.org/10.1016/j.coastaleng.2011.05.007

Camus P, Mendez FJ, Medina R, Cofiño AS (2011b) Analysis of clustering and selection algorithms for the study of multivariate wave climate. Coastal Engineering 58:453-462. https://doi.org/10.1016/j.coastaleng.2011.02.003.

Cea L, Blade E (2015) A simple and efficient unstructured finite volume scheme for solving the shallow water equations in overland flow applications. Water Resources Research 51(7):5464–5486. https://doi.org/10.1002/2014WR016547

Cea L, French JR (2012) Bathymetric error estimation for the calibration and validation of estuarine hydrodynamic models. Estuarine, Coastal and Shelf Science 100: 124-132. https://doi.org/10.1016/j.ecss.2012.01.004

Dastorani MT, Afkhami H, Sharifidarani H, Dastorani M (2010) Application of ANN and ANFIS Models on Dryland Precipitation Prediction (Case Study: Yazd in Central Iran). Journal of Applied Sciences 10: 2387-2394. https://doi.org/10.3923/jas.2010.2387.2394

Davies JL (1964) A morphogenic approach to world shorelines. Zeitschrift fur Geomorphologie 8:127-142

Duarte P, Alvarez-Salgado XA, Fernández-Reiriz MJ, Piedra S, Labarta U (2014) A modeling study on the hydrodynamics of a coastal embayment occupied by mussel farms (Ria de Ares-Betanzos, NW Iberian Peninsula). Estuarine, Coastal and Shelf Science 147:42–55. https://doi.org/10.1016/j.ecss.2014.05.021

Ellis WH, Gray DM (1966) Interrelationships between the peak instantaneous and average daily discharges of small prairie streams. Canadian Agricultural Engineering

Fraga I, Cea L, Puertas J, Suárez J, Jiménez V, Jácome A (2016) Global sensitivity and GLUE-based uncertainty analysis of a 2D-1D dual urban drainage model. Journal of Hydrologic Engineering 21(5):04016004

Fraga I, Cea L, Puertas J (2017) Validation of a 1D-2D dual drainage model under unsteady part-full and surcharged sewer conditions. Urban Water Journal 14(1):74-84

Franke R (1982) Scattered data interpolation: tests of some methods. Math. of Comp. 38:181–200. https://doi.org/10.1090/S0025-5718-1982-0637296-4

Fuller WE (1914). Flood Flows. Trans. Amer. Soc. Civil Engrs. 77:564- 617

Garrity NJ, Battalio R, Hawkes PJ, Roupe D (2006) Evaluation of the event and response approaches to estimate the 100-year coastal flood for Pacific coast sheltered waters. Proc. 30th ICCE, ASCE, 1651–1663. https://doi.org/10.1142/9789812709554_0140

Garrote J, Alvarenga FM, Díez-Herrero A (2016) Quantification of flash flood economic risk using ultra-detailed stage–damage functions and 2D hydraulic models. Journal of Hydrology 541:611-625. https://doi.org/10.1016/j.jhydrol.2016.02.006

Hanson H, Larson M (2008) Implications of extreme waves and water levels in the southern Baltic Sea. Journal of Hydraulic Research 46:sup2, 292-302. https://doi.org/10.1080/00221686.2008.9521962

Hawkes PJ (2003) Extreme Water Levels in Estuaries and Rivers The combined influence of tides, river flows and waves. DEFRA Defra/Environment Agency. R&D Technical Report FD0206/TR1. HR Wallingford Report SR 645

Hawkes PJ, Gouldby BP, Tawn JA, Owen MW (2002) The joint probability of waves and water levels in coastal engineering design. J. Hydraul. Res. 40:241–251. https://doi.org/10.1080/00221680209499940

Hawkes PJ (2008) Joint probability analysis for estimation of extremes. Journal of Hydraulic Research 46(2): 246-256. https://doi.org/10.1080/00221686.2008.9521958

Hayes MO (1979) Barrier island morphology as a function of tidal and wave regime. Barrier Islands - from the Gulf of St. Lawrence to the Gulf of Mexico:1-27

IH Cantabria (2014) Extreme events hydrograph characterization at Galicia coast watershed. Department of Water Planning Administration of the Galician Government (in Spanish)

Kennard RW, Stone LA (1696) Computer aided design of experiments. Technometrics 11(1):137-148. https://doi.org/10.2307/1266770

Kirpich ZP (1940) Time of concentration of small agricultural watersheds. Civil Engineering 10(6):362

Mazas F, Hamm L (2017) An event-based approach for extreme joint probabilities of waves and sea levels. Coastal Engineering 122:44-59

Perez-Gomez B (2014) Design and implementation of an operational sea level monitoring and forecasting system for the Spanish coast. PhD Thesis, University of Cantabria

Petroliagkis TI, Voukouvalas E, Disperati J, Bildot J (2016) Joint Probabilities of Storm Surge, Significant Wave Height and River Discharge Components of Coastal Flooding Events. EUR 27824 EN. https://doi.org/10.2788/677778

Roe PL (1986) Discrete models for the numerical analysis of time-dependent multidimensional gas dynamics. Journal of Computational Physics 63:458–476

Robson A, Reed R (1999) Flood Estimation Handbook, vol. 3, Statistical Procedures for Flood Frequency Estimation, Wallingford HydroSolutions, Wallingford, UK

Rueda A, Vitousek S, Camus P, Tomás A, Espejo A, Losada IJ et al (2017) A global classification of coastal flood hazard climates associated with large-scale oceanographic forcing. Scientific Reports 7(1):5038

Svensson C, Jones DA (2002) Dependence between extreme sea surge, river flow and precipitation in eastern Britain. Int. J. Climatol. 22:1149-1168

Svensson C, Jones DA (2004) Sensitivity to storm track of the dependence between extreme sea surges and river flows around Britain. In: Hydrology: Science and Practice for the 21st Century, Vol. 1, Proc. From the British Hydrological Society's international conference, London, UK. 239a-245a.

Taguas EV., Ayuso JL, Pena A, Yuan Y, Sanchez MC, Giraldez JV, Perez R (2008) Testing the Relationship between Instantaneous Peak Flow and Mean Daily Flow in a Mediterranean Area Southeast Spain. Catena 75:129–137. https://doi.org/10.1016/j.catena.2008.04.015

Teakle I, Gildas C, Khondker R, Breen M, McGarry D (2005) Boundary conditions for estuarine flood modelling using joint probability analysis, Proc. of Coasts and Ports: Coastal Living – Living Coast, Australasian Conference: 613–619

Temez JR (1991) Extended and improved Rational Method. Proc. XXIV Congress of IAHR, Madrid, España. Vol. A. pp 33-40

Thieken A, Merz B, Kreibich H, Apel H (2006) Methods for flood risk assessment: Concepts and challenges. International Workshop on Flash Floods in Urban Areas. Muscat – Sultanate of Oman.

Van Gelder PHAJM, Vrijling JK, Van Haarden DH (2004) Joint probability distribution for wave height, wind setup and wind speed. 29th Int. Coastal Engineering, Lisbon, 1032-1046

Van der Made, JW (1969) Design levels in the transition zone between the tidal reach and the river regime reach, Hydrology of Deltas, Vol. 2 of Proceedings of the Bucharest Symosium, May, 1969, 246–257

Wadey MP, Brown JM, Haigh ID, Dolphin T, Wisse P (2015) Assessment and comparison of extreme sea levels and waves during the 2013/14 storm season in two UK coastal regions. Nat. Hazards Earth Syst. Sci., 15, 2209–2225. https://doi.org/10.5194/nhess-15-2209-2015

Webster T, McGuigan K, Collins K, MacDonald C. 2014. Integrated River and Coastal Hydrodynamic Flood Risk Mapping of the LaHave River Estuary and Town of Bridgewater, Nova Scotia, Canada. Water 6: 517-546. https://doi.org/10.3390/w6030517

While CJ (2007) The use of joint probability analysis to predict flood frequency in estuaries and tidal rivers. University of Southampton, School of Civil Engineering and the Environment, Doctoral Thesis

Yu GH, Huang CC (2001) A distribution free plotting position. Stochastic environmental research and risk assessment 15(6): 462-476

Zhong H, Van Overloop PJ, Van Gelder PHAJM (2013) A joint probability approach using a 1D hydrodynamic model for estimating high water level frequencies in the Lower Rhine Delta. Nat. Hazards Earth Syst. Sci. 13:1841–1852. https://doi.org/10.5194/nhess-13-1841-2013

Figures and Tables

Fig. 1 Schematic representation of the main steps of the proposed methodology

Fig. 2 Betanzos estuary (top). Map of Betanzos city in the 14th century (Colón 2012) (bottom-left) and schematic representation of the urbanisation and land uses in 2016 (bottom-right)

Fig. 3 Monthly average and standard deviation values of daily tidal range TR (top-left), mean daily discharge Q_d (top-center) and mean daily storm surge S_d (top-right), and correlations between these predictors (bottom)

Fig. 4 Correlation coefficient between Q_d and S_d computed on a monthly basis (left), Qd-Rd scatter plot for the months of January (center) and June (right). Values computed from historical and synthetic data are shown in blue and red respectively

Fig. 5 Regression between the observed mean daily discharges at the gauging stations of the Mandeo (Qmandeo) and Mendo (Qmendo) rivers. The synthetic values of the Mendo discharge computed from Equation (1) and the fitted power regression are also shown

Fig. 6 Relation between Q_p and Q_d at Mandeo gauging station (left). The fitted 2-branch power regression curve is shown as a solid line. Comparison between measured and estimated SCS hydrographs at the Mandeo gauge station for a flood event (rigt)

Fig. 7 Spatial domain included in the 2D inundation model, including the confluence of the rivers Mandeo and Mendo, and the estuary of Betanzos. Imposed boundary conditions are also shown schematically. Control points (bottom-left) and detail of the numerical mesh (top-left)

Fig. 8 Water levels referred to the Mean Sea Level at the Alicante tide gauge (Spain) for different return periods computed with the proposed methodology at control points 1, 3, 9 and 12. The water levels computed with the standard methodology for the return periods of 2.33, 100 and 500 years are also shown

Fig. 9 Inundation maps for the return period of 2.33 years computed with the proposed methodology (light blue) and with the standard methodology (dark blue)

Fig. 10 Longitudinal profile along the rivers Mendo and Mandeo of the 100-year return period water level computed with the proposed and the standard methodologies

Fig. 11 Validation of the water level reconstruction methodology (Radial Basis Function). Water levels simulated with the numerical model Iber and reconstructed with the RBF technique at control points 8 (left) and 9 (right) for 20 validation cases.

Table 1 Relation between return periods computed with the standard and proposed methodologies at several control points. The location of the control points is shown in Fig. 7

Standard methodology (years)	**Proposed methodology (years)**											
	CP 1	**CP 2**	**CP 3**	**CP 4**	**CP 5**	**CP 6**	**CP 7**	**CP 8**	**CP 9**	**CP 10**	**CP 11**	**CP 12**
2.33	10	10	5	4	4	3.5	3	3	5	3	3	3
100	>500	>500	500	500	500	500	300	200	>500	>500	400	100
250	>500	>500	>500	>500	>500	>100	250	250	>500	>500	500	250

Figure01

Click here to download Figure Fig01_174mm01.jpg

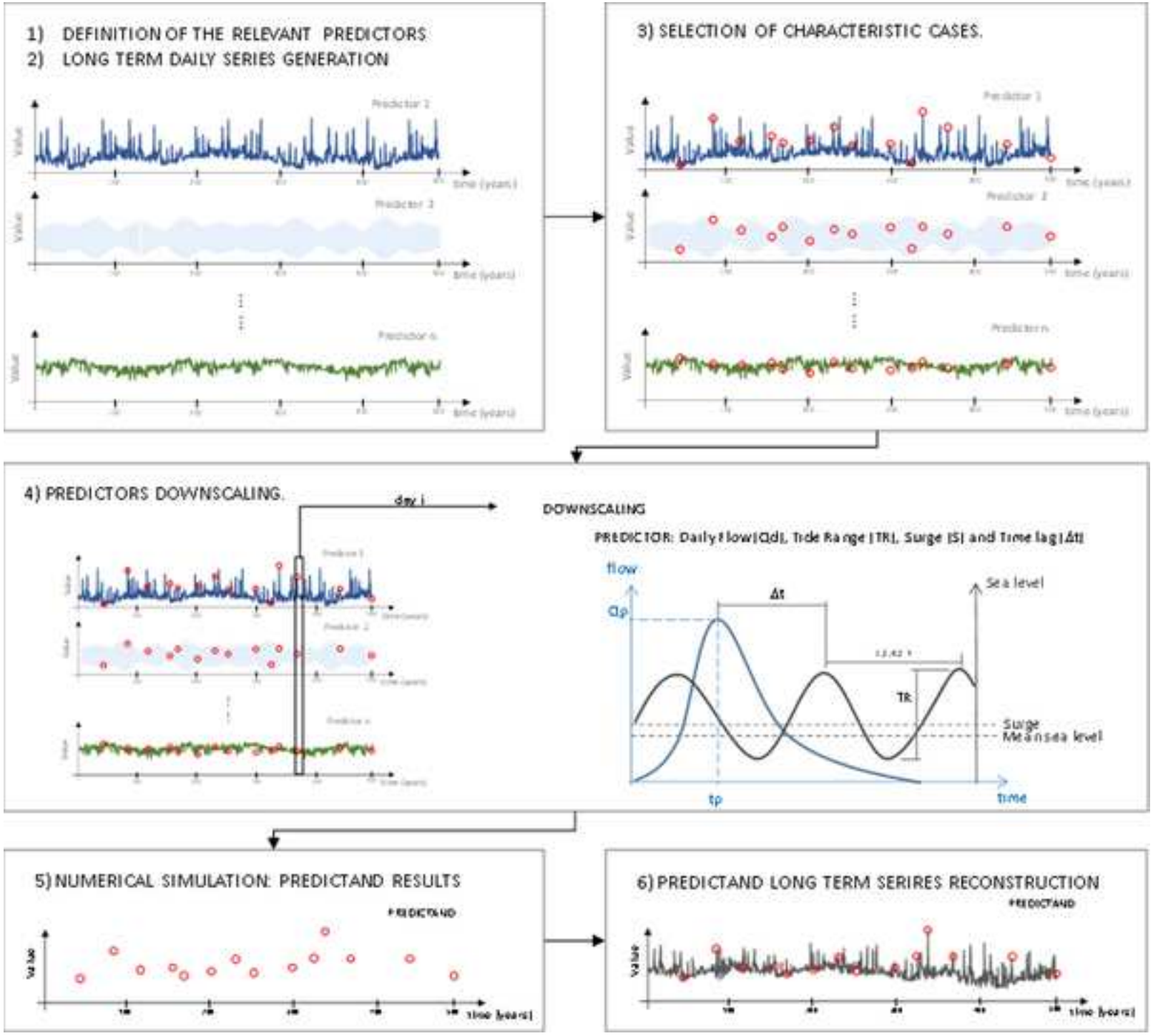

Figure02

Click here to download Figure Fig02_174mm01.jpg

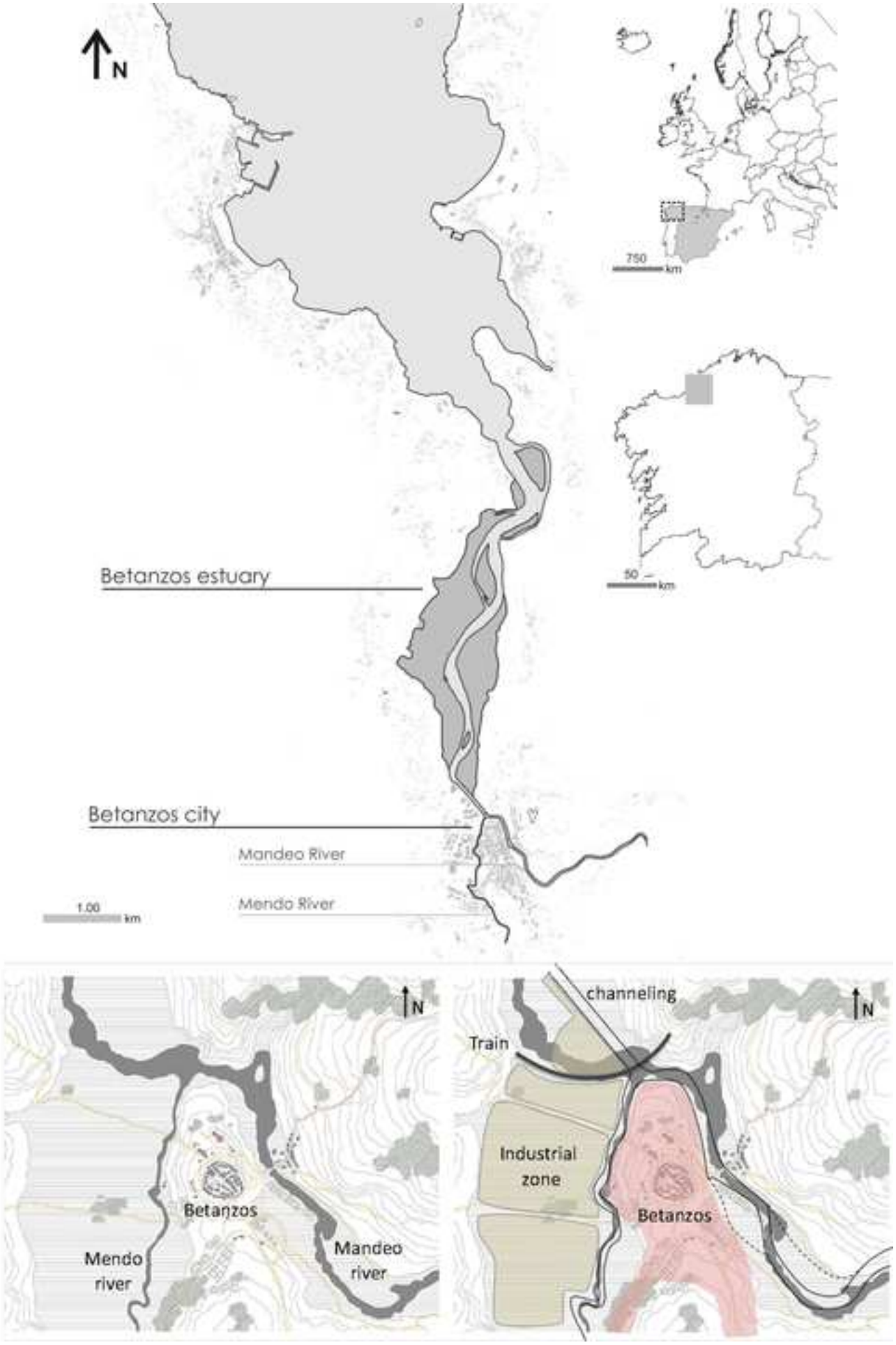

Figure03

Click here to download Figure Fig03_129mm01.jpg

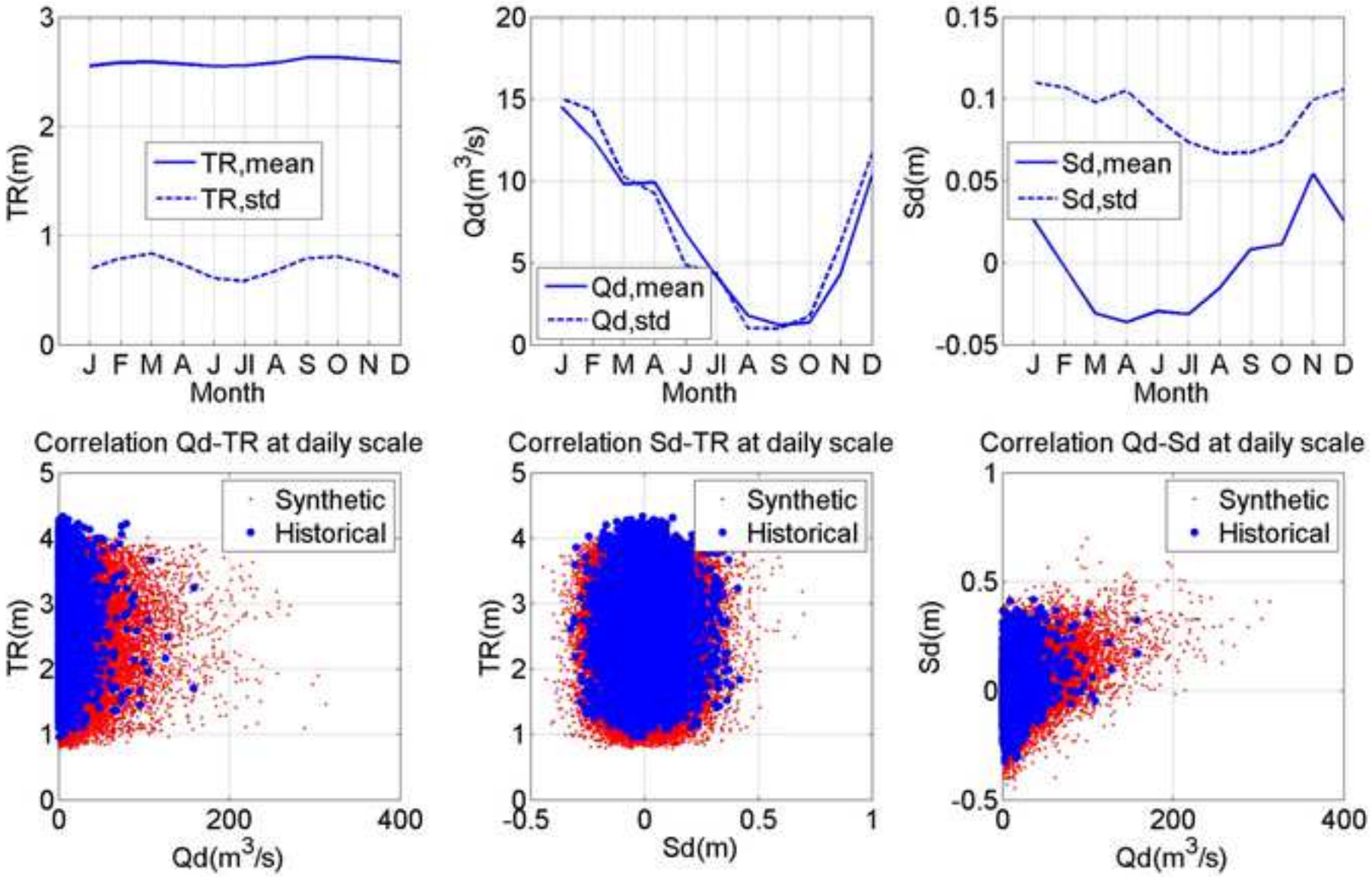

Figure04

Click here to download Figure Fig04_129mm01.jpg

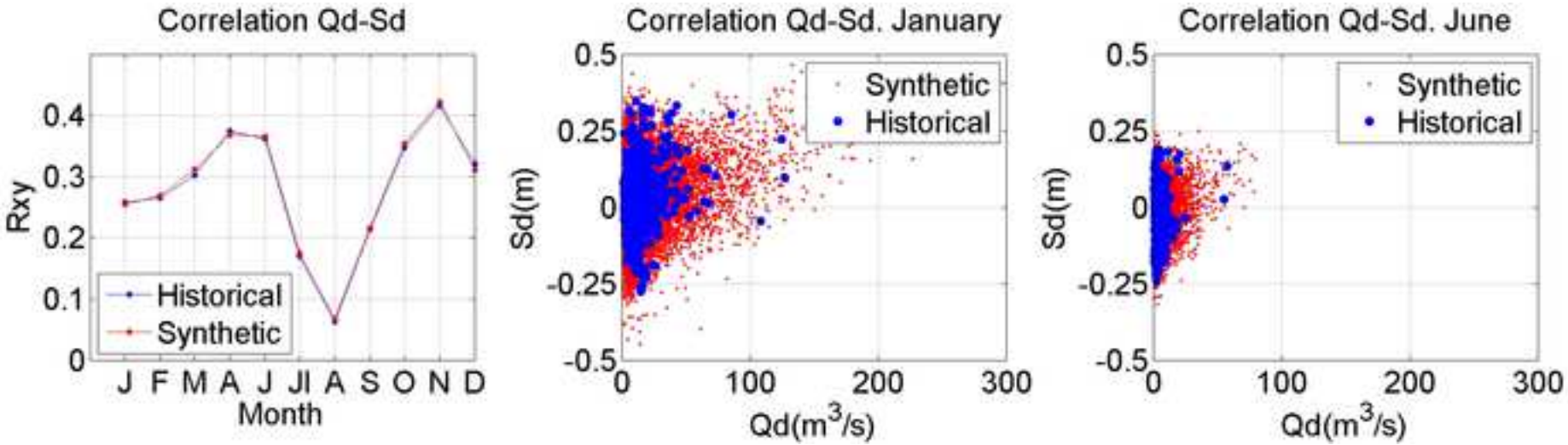

Figure05

Click here to download Figure Fig05_84mm01.jpg

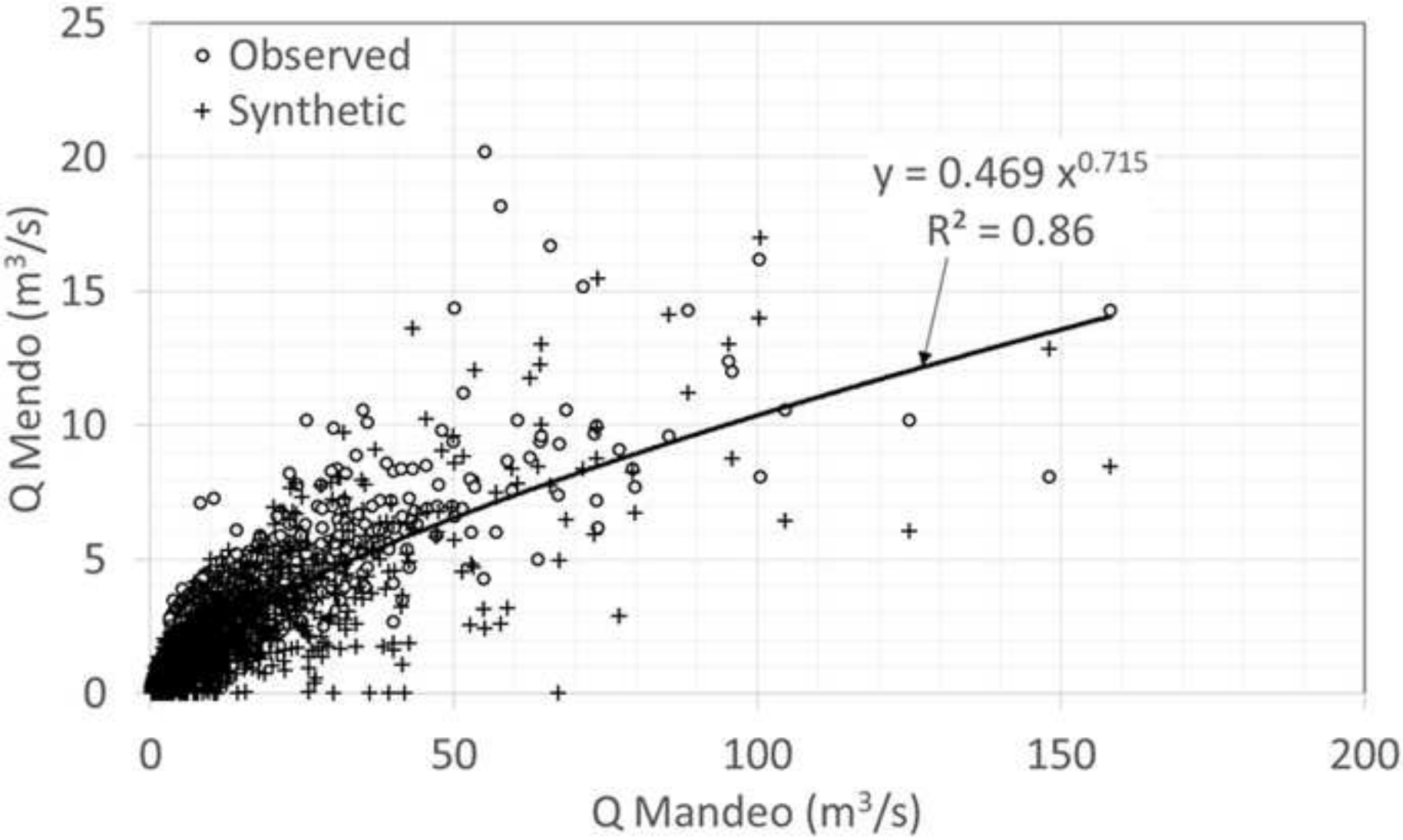

Figure06

Click here to download Figure Fig06_174mm01.jpg

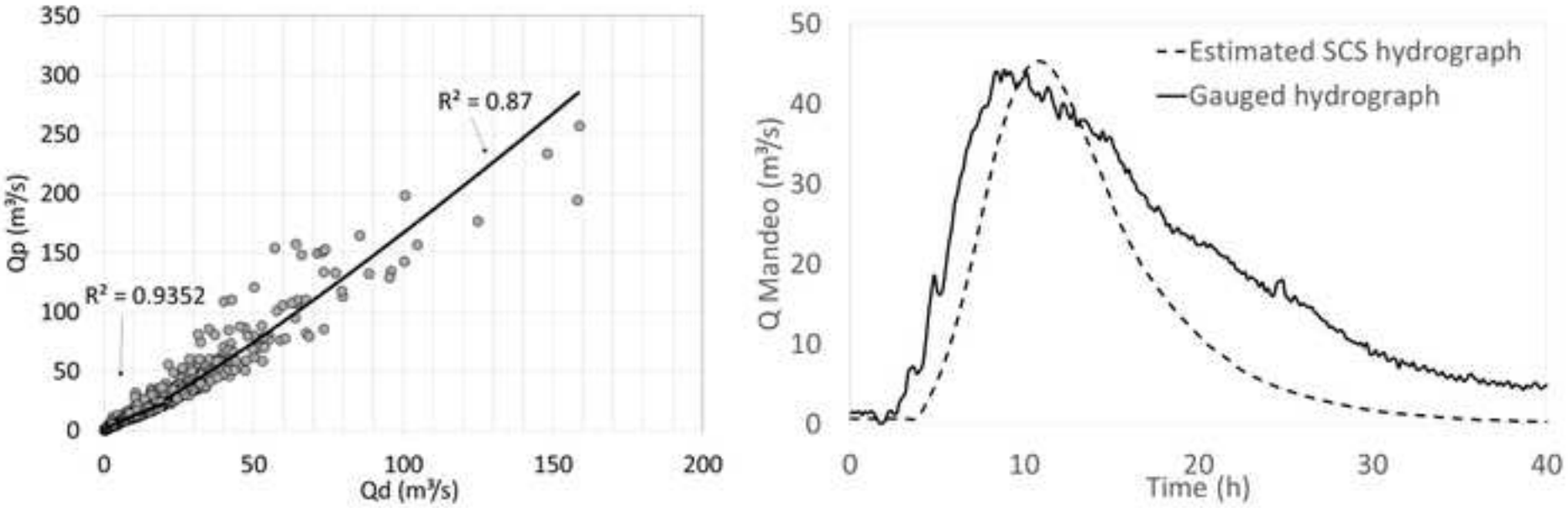

Figure07

Click here to download Figure Fig07_174mm01.jpg

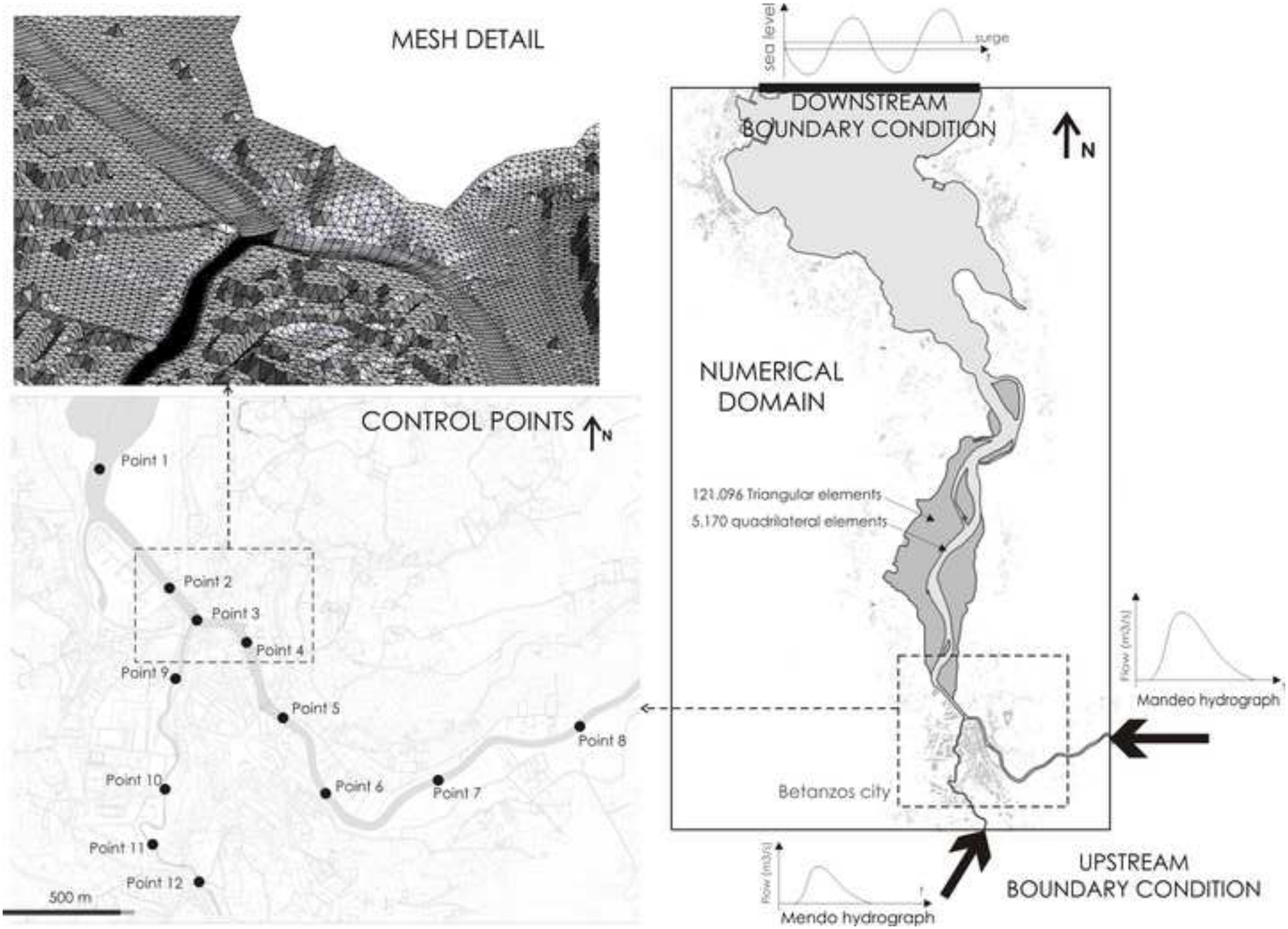

Figure08

Click here to download Figure Fig08_174mm01.jpg

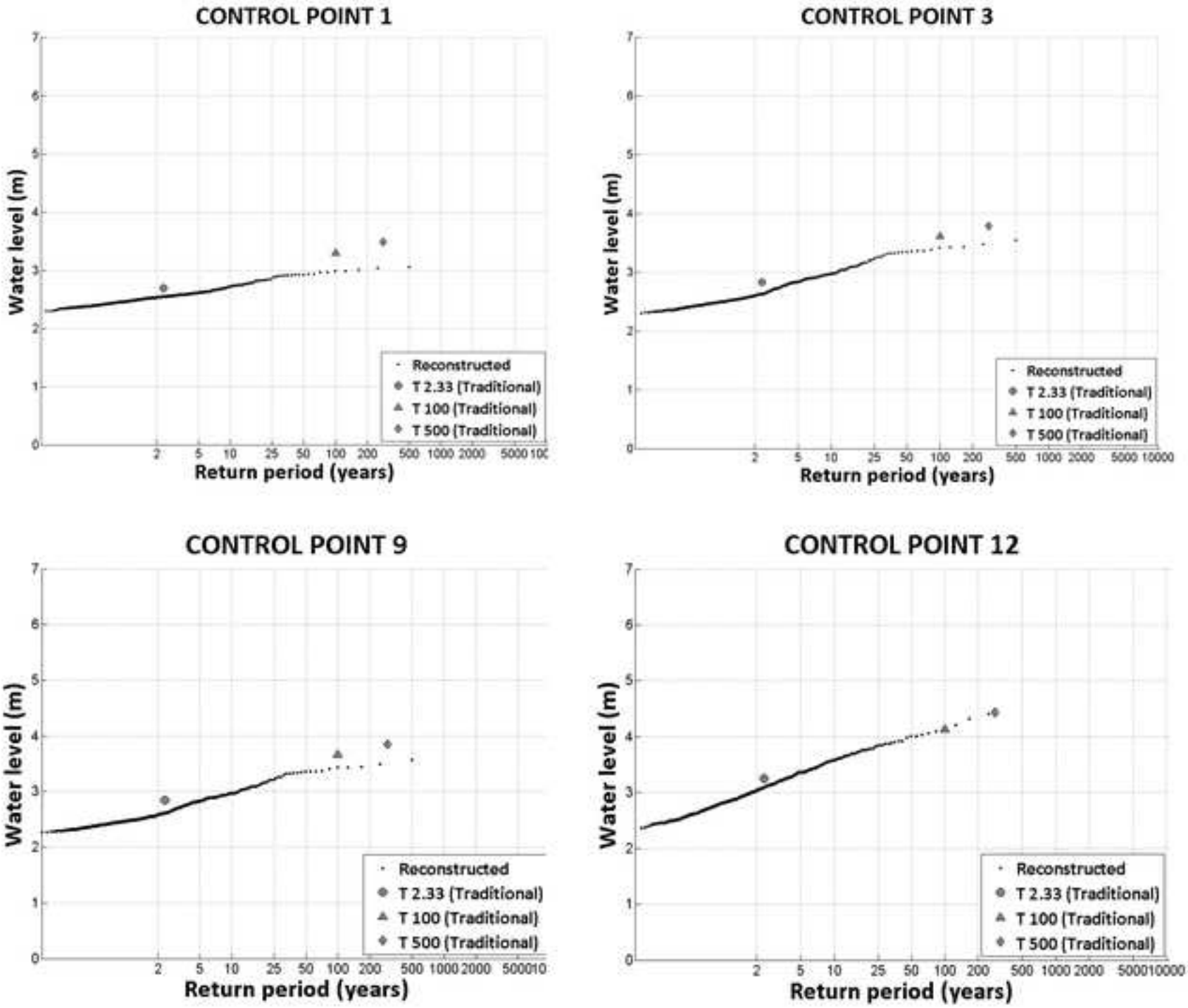

Figure09

Click here to download Figure Fig09_174mm01.jpg

Figure10

Click here to download Figure Fig10_122mm01.jpg

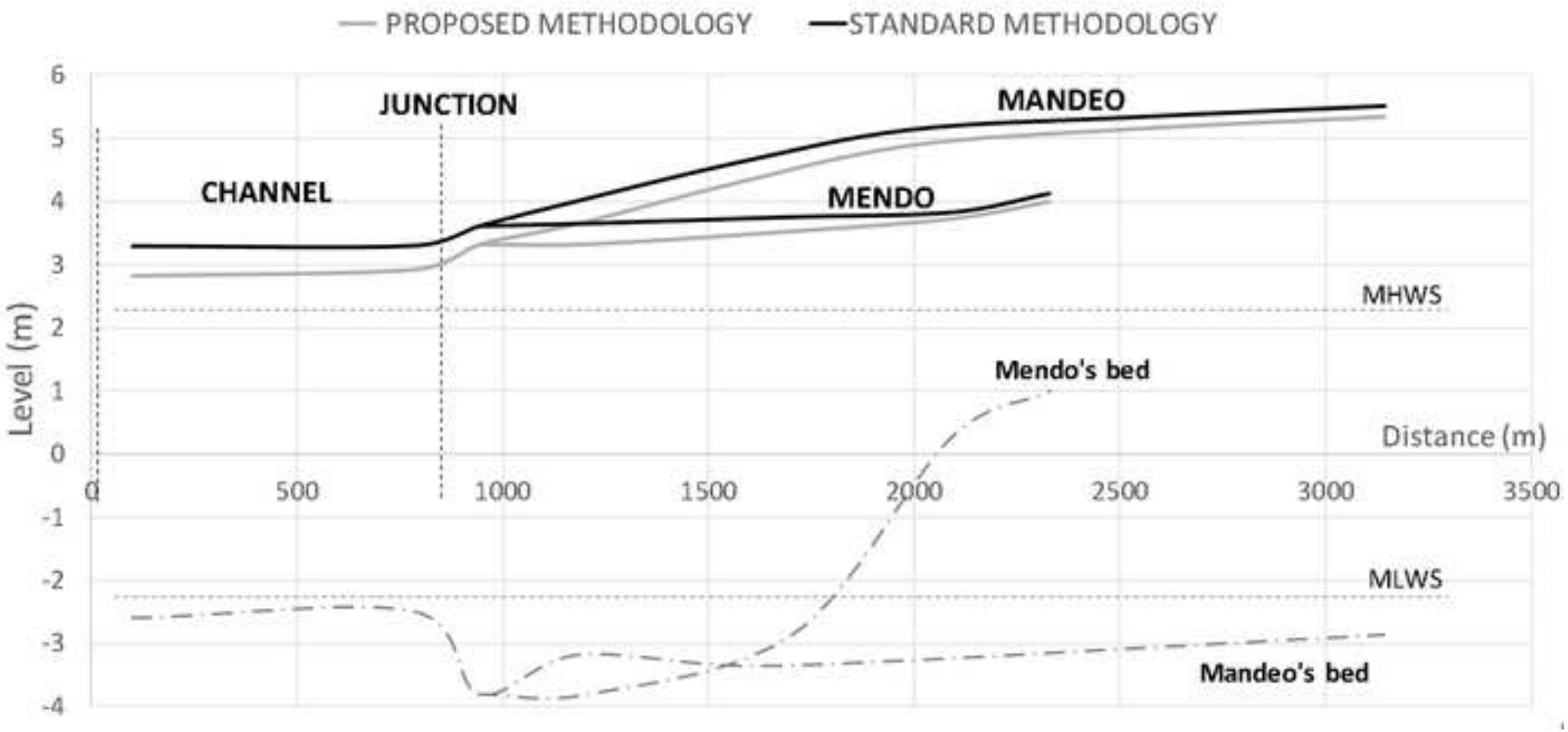

Figure10

Click here to download Figure Fig11_174mm01.jpg

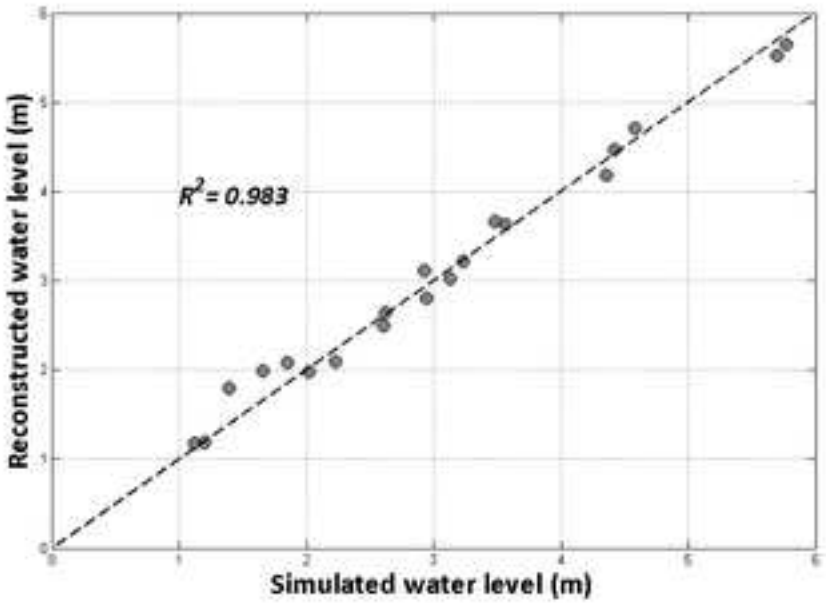

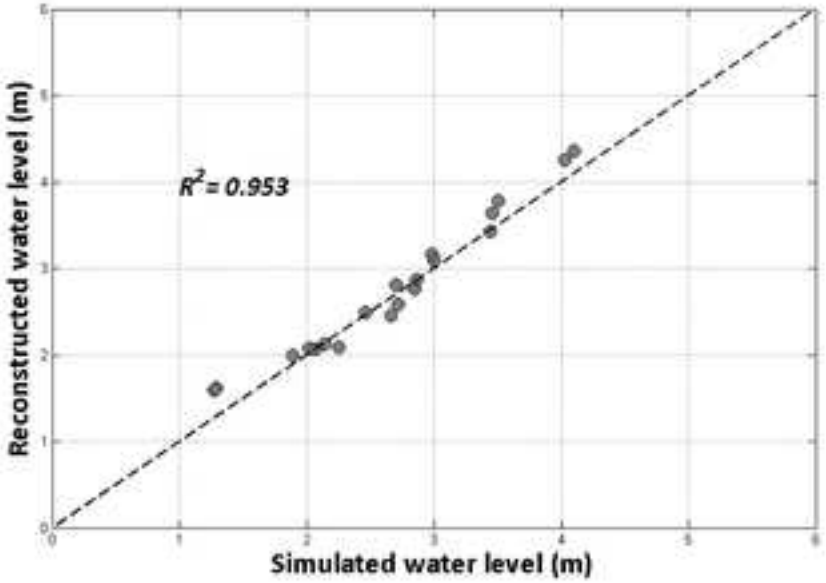

Control Point	CP 1	CP 2	CP 3	CP 4	CP 5	CP 6	CP 7	CP 8	CP 9	CP 10	CP 11	CP 12
R^2	0.91	0.93	0.94	0.94	0.95	0.96	0.98	0.98	0.95	0.91	0.91	0.94